High Q Coil Measurement for Inductive Power Transfer

James Lawson, David C. Yates, *Member, IEEE*, and Paul D. Mitcheson, *Senior Member, IEEE*

***Abstract*— A system for the measurement of quality factors, self-inductances, and interturn capacitances of inductive power transfer coils, in the frequency range of 1–20 MHz, is demonstrated. Coil quality factor in excess of 1000 is measured at megahertz frequencies, beyond the capabilities of commercial impedance analyzers. The method used is to measure the transmission bandwidth of the coil under test while under weak magnetic coupling, incorporating measures to reduce common-mode coupling. The measurement system is verified by comparison with electromagnetic simulation and by modeling. The system model shows robustness to system configuration and the potential to measure coils with Q in excess of 10 000.**

***Index Terms*— Capacitance, coil measurement, inductance, inductive power transmission, Q-factor, wireless power.**

I. Introduction

INDUCTIVE power transfer (IPT) is a method of delivering power to a remote load using magnetic fields. Energy is wirelessly coupled from a transmitter coil to a resonant receiver coil. The space between the coils can be filled with dielectric (e.g., air) or partially conductive media (e.g., tissue). IPT can efficiently provide power to remote loads over distances comparable to the constituent coils' diameters [1]. A complete IPT system (Fig. 1) is usually used to transfer power from a dc power source to a dc load and thus includes power electronic converters; however, this paper addresses only the inductive link between the coils. Commonly, in the frequency range focused on this paper (1–20 MHz), the coils are simple, air cored, loosely wound inductors of helical [2] or planar spiral form [3].

In recent years, many IPT systems have been demonstrated operating at the industrial, scientific, and medical (ISM) frequencies of 6.78 MHz [2], 13.56 MHz [4], and 27 MHz [5], with end-to-end efficiencies over 70%. These megahertz frequencies are attractive for the operation of air-core coils as they, for many common applications, yield the greatest possible link efficiency, η. Furthermore, ISM frequencies do not require licensing to use worldwide.

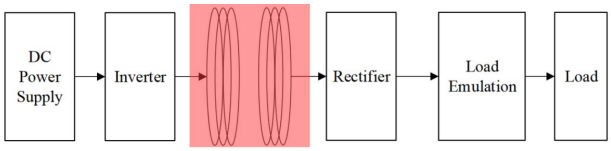

Fig. 1. Block diagram of a complete IPT system, with the inductive link highlighted.

High link efficiency is only possible for systems when the transmitter and receiver coils have high quality factor, Q, [1]. Systems operating without coupling factor enhancing materials quality factors' approach and, in some cases, exceed 1000 [6]. Direct measurement of coil Q greater than 30 is challenging [7], due to the requirement to accurately measure a small loss in the presence of a large reactance. The difficulty in obtaining reliable Q data for ISM band IPT has, despite the importance of coil loss in efficiency calculations, resulted in many publications only stating end-to-end efficiency measurements and not measured coil losses [8], [9]. Where coils are measured, the quality factors are frequently found to be less than expected even for modest Q [10]. As a result, there is ambiguity about where losses are arising in systems. The aim of this paper is to report on a system that can reliably measure coil Q in excess of 1000 in ISM bands. Furthermore, coil Q can be determined by the system at frequencies where radiation is the dominant loss mechanism. Conventional impedance analyzers are compared with the system. They are found not to be able to accurately measure the coil properties when Q is high or return meaningful results when the radiation loss is significant. The measurement system has been verified by both the measurement of simulated coils and by equivalent circuit modeling. The system model is used to show the operating principles and the limitations of the measurement system.

A. Link Efficiency

The link efficiency, η, is the efficiency of the magnetic link including losses in coils and media. As it does not include power electronic losses and assumes an optimal receiver coil load, it is an upper bound on overall end-to-end efficiency of an IPT system. A wireless power transfer system, inclusive of media losses, can be regarded as a two-port network, for

Manuscript received May 4, 2018; revised November 25, 2018; accepted January 17, 2019. Date of publication March 25, 2019; date of current version May 6, 2019. The work of J. Lawson was supported in part by the Engineering and Physical Sciences Research Council (EPSRC) and in part by the Électricité de France (EDF) through Industrial Cooperative Awards in Science and Technology (CASE) Award Voucher 11220474. The work of D. C. Yates was supported in part by the EPSRC U.K.–China: Interface and Network Infrastructure to Support EV Participation in Smart Grids under Grant EP/L00089X/1 and in part by the EPSRC Underpinning Power Electronics 2012: Components Theme under Grant EP/K034804/1. *(Corresponding author: James Lawson.)*

J. Lawson is with the Nuclear Physics Group, STFC Daresbury Laboratory, Warrington WA4 4AD, U.K. (e-mail: james.lawson@stfc.ac.uk).

D. C. Yates and P. D. Mitcheson are with the Control and Power Research Group, Electrical and Electronic Engineering Department, Imperial College London, London SW7 2AZ, U.K. (e-mail: david.yates@imperial.ac.uk; paul.mitcheson@imperial.ac.uk).

Color versions of one or more of the figures in this paper are available online at http://ieeexplore.ieee.org.

Digital Object Identifier 10.1109/TMTT.2019.2901442

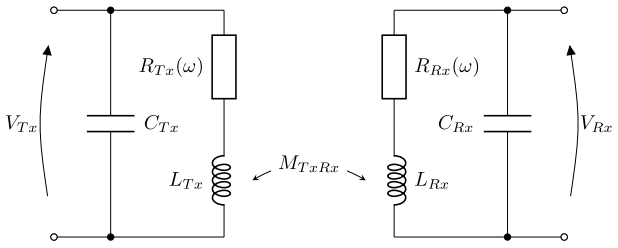

Fig. 2. Transformer model of IPT system, with parasitic capacitances and frequency-dependent loss resistance.

which the generalized efficiency has been solved by Zargham and Gulak [11]

$$x = \frac{|Z_{21}|^2}{\mathrm{Re}(Z_{11})\,\mathrm{Re}(Z_{22}) - \mathrm{Re}(Z_{12})^2} \tag{1}$$

$$\eta = \frac{x}{(1+\sqrt{1+x})^2}. \tag{2}$$

In a purely inductively coupled system (Fig. 2), without media losses, x, reduces to the familiar equation

$$x = k^2 Q_{\mathrm{Tx}} Q_{\mathrm{Rx}} \tag{3}$$

and

$$k = \frac{M_{\mathrm{TxRx}}}{\sqrt{L_{\mathrm{Tx}} L_{\mathrm{Rx}}}} \tag{4}$$

where M_{TxRx} is the mutual inductance between the transmitter and receiver coils and L_{Tx} and L_{Rx} are their self-inductances. It is critical to accurately determine coil Q in order to use the link efficiency equation to predict the performance of an IPT system.

B. Q Requirements for Coreless IPT Systems

To illustrate the importance of Q-factors approaching 1000 in practical applications, an example is now presented. In this example, simplified geometry is used to show the typical efficiency against distance curves for coil Q from 100 to 1000.

The self, $L_{\mathrm{Tx,Rx}}$, and mutual inductance, M_{TxRx},of two identical loops of 150-mm outer radius, r_{Max}, composed of 5 mm radius, a, wire has been calculated for coaxial center-to-center distances, D, from 0.05 to 0.6 m. The inductances are used to calculate the coupling factor between the two loops. The formula [12]

$$L_{\mathrm{Tx,Rx}} \cong \mu_0 r_{\mathrm{Max}} \left(\ln\left(\frac{8 r_{\mathrm{Max}}}{a}\right) - 2 \right), \quad r_{\mathrm{Max}} \gg a \tag{5}$$

is used to calculate the self-inductance of the loops. The formula [13]

$$M_{\mathrm{TxRx}} = f(\tau^2) r_{\mathrm{Max}} (1 \times 10^{-6}) \tag{6}$$

$$\tau^2 = \frac{(D(1\times 10^2))^2}{4(r_{\mathrm{Max}}(1\times 10^2))^2 + (D(1\times 10^2))^2} \tag{7}$$

where $f(\tau^2)$ is calculated using linear interpolation of the table in [13, pp. 79 and 80]. The link efficiency with respect to distance is then compared for coils of varying Q using (2) resulting in (Fig. 3).

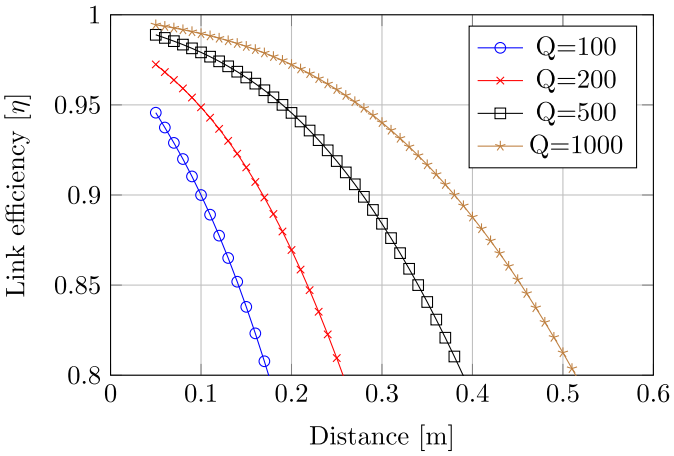

Fig. 3. Case study of effect on coil Q on inductive link efficiency.

If an overall system efficiency of 85% is targeted, it is reasonable to expect $\eta > 0.9$ to allow a minimal budget for power electronic losses. It is observed that the point of $\eta = 0.9$ increases from 0.1 to 0.38 m when Q is increased from 100 to 1000, a significant increase in distance that enables applications such as wireless car charging. With similar dimensions, coils have been demonstrated with Q in excess of 1000 at megahertz ISM frequencies [6], [14].

C. Q Definitions

For proper discussion of coil Q, the approximations of the coil model (Fig. 2) and the multiple applicable definitions of Q are now discussed.

1) Loss Relocation: For ease of discussion of the unloaded coil Q, the circuit can be transformed from a series L and R to a parallel circuit. New parallel equivalent values for the coil loss, $R'(\omega)$ and for the coil inductance, L' are defined such that the parallel network has the same input impedance as the individual unloaded coils

$$R'(\omega) = \frac{R(\omega)^2 + L^2\omega^2}{R(\omega)} \tag{8}$$

$$L' = \frac{R(\omega)^2 + L^2\omega^2}{L\omega^2}. \tag{9}$$

2) Energy Definition: Q is only formally defined at resonance, ω_0, as

$$Q = 2\pi \frac{E_s}{E_d} \tag{10}$$

where E_s is the peak stored energy in the resonator and E_d is the energy lost per resonant cycle [15]. When Q of a lossy capacitor or inductor is stated, it is implicitly resonating with a lossless inductor or capacitor, respectively. The voltage across the parallel resonator (Fig. 4) is common to all components

$$v(t) = |V| \cos(\omega_t). \tag{11}$$

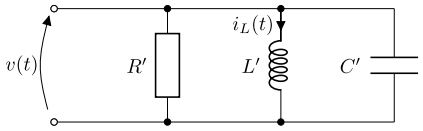

Fig. 4. Parallel LCR resonator.

The electrical energy stored in the capacitor, E_e, follows from definition:

$$E_e(t) = \frac{C}{2}|V|^2\cos^2(\omega t). \tag{12}$$

To calculate the magnetic energy, E_m, stored in the inductor, first, the inductor current is calculated

$$i_L(t) = \frac{1}{L}\int v(t)dt = \frac{|V|}{\omega L}\sin(\omega t) \tag{13}$$

$$E_m(t) = \frac{1}{2}Li_L(t)^2 = \frac{|V|^2}{2\omega^2 L}\sin^2(\omega t). \tag{14}$$

By equating the peak magnetic and electric energies, the familiar expression for the resonant frequency can be derived as

$$\frac{|V|^2}{2\omega^2 L} = \frac{1}{2}C|V|^2 \therefore \omega_0 = \frac{1}{\sqrt{LC}}. \tag{15}$$

To calculate the energy lost per resonant cycle, E_d, first, the instantaneous power loss is defined

$$P_d(t) = \frac{v(t)^2}{R} \tag{16}$$

$$E_d = \int_0^{\frac{2\pi}{\omega_0}} P_d(t)dt = \frac{|V|^2}{R}\int_0^{\frac{2\pi}{\omega_0}} \cos^2(\omega_0 t)dt = \frac{\pi|V|^2}{R\omega_0}. \tag{17}$$

Finally, the Q-factor of the parallel resonator can be calculated as

$$Q = 2\pi\left(\frac{|V|^2}{2\omega_0^2 L}\right)\left(\frac{R\omega_0}{\pi|V|^2}\right) = \frac{R}{\omega_0 L}. \tag{18}$$

This Q-factor is defined at a single resonant frequency and, therefore, is not affected by the change in resistance with respect to frequency caused by the skin and radiation (dispersion).

3) Bandwidth Definition: If the parallel resonator (Fig. 4) is considered to be excited by a current source, the two angular frequencies at which the power dissipated in the resonator is −3 dB referenced to the maximum power dissipated in the resonator are

$$|Z(\omega_{-3dB})| = \frac{R}{2} \tag{19}$$

$$\omega_{-3dB} = \frac{\sqrt{2}\sqrt{L^2 + 2CR^2L \pm \sqrt{L^4 + 4L^3CR^2}}}{2CRL}. \tag{20}$$

An alternative definition of Q is

$$Q_{-3dB} = \frac{\omega}{\Delta\omega} \tag{21}$$

where $\Delta\omega$ is the −3-dB bandwidth of the resonator, this definition is not identical to the energy definition. The usage of this definition in the measurement of IPT coils has the difficulty that R is a function of ω and, therefore, will have varied within the resonator bandwidth (dispersion).

However, for Q greater than 10 (all IPT coils), the bandwidth and energy definitions can be considered equivalent. In the Appendix, this has been verified under dispersive conditions by computer modeling.

D. Factors Affecting Q

The mechanisms of the ac losses in a coil (Fig. 2), represented by R are resistive losses due to the current distribution in the turns and radiation loss caused by far-field radiated energy. The total loss resistance can be split into separate losses [16]

$$R = R_{\text{rad}} + R_{\text{skin}}G_p \tag{22}$$

where R_{rad} is the coil's radiation resistance, R_{skin}, is an isolated conductors skin effect resistance, and G_p is the proximity factor.

An approximation to the skin effect resistance of an electrically thick tube of outer radius, a, in terms of length, l, is [17]

$$R_{\text{skin}} = \frac{l}{2\pi a}\sqrt{\frac{\omega\mu}{2\sigma}}. \tag{23}$$

Therefore, $R_{\text{skin}} \propto \omega^{0.5}$ by comparison with (18), it is observed that at low frequencies where the skin effect resistance is dominant $Q \propto \omega^{0.5}$.

The radiation resistance of simple structures such as wire loops (magnetic dipole) can be calculated analytically; however, expressions do no generally exist for more complex structures. Therefore, the solution for the magnetic dipole is used to approximate the radiation resistance of more complex coils by assuming each turn is a layered magnetic dipole [18]

$$R_{\text{rad}} = \left(\frac{377}{6\pi}\right)\left(\frac{2\pi}{\lambda}\right)^4 (N\pi r^2)^2 \tag{24}$$

where r is the mean turn radius. As $R_{\text{rad}} \propto \omega^4$ and $R_{\text{skin}} \propto \omega^{0.5}$, the point of maximum Q will lie at a frequency where $R_{\text{rad}} < R_{\text{skin}}$ where the radiated energy from the magnetic link is small. It can be assumed that the phase velocity in the coil is the speed of light as they are electrically small.

The proximity factor takes into account the increase in resistance due to current redistribution caused by other turns in the coils cross section. In an IPT coil, due to the skin effect, it is a reasonable assumption that the turns are electrically thick, and as such, the coil current flows entirely on the outside of the conductor. With this assumption, the proximity factor will be constant with respect to frequency.

E. Full Wave EM Simulation Considerations

When IPT coils are modeled in electromagnetic (EM) simulation package results that are directly comparable with measurements are not obtained by the use of default settings. Correct fitting to the coil model (Fig. 2) and unusually accurate simulation settings are required to obtain correct results.

1) Electrical Effects: When conducting full-wave EM simulations of IPT coils to determine their Q electrical and magnetic effects are simulated. A real IPT coil unlike the model (Fig. 2) has electrical length, the electrical length effects cause multiple resonant frequencies. To fit the coil model, the simulation results should be truncated before the first resonant frequency as to avoid subsequent resonances.

When measuring the coil with a resonant method, the coils' inductive reactive impedance is the additive inverse of the resonating capacitors, for nonresonant methods such as single-port S-parameters from an EM simulator's complex coil impedance, Z_{11}, which is obtained directly. The problem of fitting the coil model (Fig. 2) to the impedance data then arises. In the model of the coil, it is assumed that the effective inductance of the coil and the effective capacitance of the coil do not vary with frequency, however, the loss resistance $R(\omega)$ is a function of frequency. If C is removed from the coil model, the imaginary impedance has a linear relationship with angular frequency. Thus, a simple overdetermined algorithm can be devised to find the capacity that fits. The following curve can be plotted from the impedance data:

$$y = \frac{1}{\omega\left(\frac{1}{\mathrm{Im}(Z_{11})} + \omega C\right)} \tag{25}$$

$$x = \omega. \tag{26}$$

The least means squares linear fit to this data is then performed. By the selection of the correct value of C, the gradient of this fit will be 0. Overestimate of C will result in a negative gradient, underestimate in a positive gradient; therefore, by the use of bisection, the estimate of C is refined through successive approximation. Once C is estimated to the required precision, the inductance of the coil is given by the y-axis intercept of the line of best fit.

2) Required S-Parameter Accuracy: The default S-parameter accuracy of CST MWS (a popular EM simulator) is 1×10^{-3}, this is insufficient to report high Q-factors. The paper of Kuhn and Boutz [7] gives a simple approximate equation to find the reflection magnitude, $|\Gamma\ |$, in relation to Q in the region $Z = +jZ_0$

$$|\Gamma\ | \approx 1 - \frac{1}{Q}. \tag{27}$$

This expression is accurate for $Q > 30$. The S-parameter accuracy of 1×10^{-6} allows reporting of Q of 1000 within the range of 999.5–1000.5, while 1×10^{-3} only allows the same Q to be reported in the range of 666.67–2000. Therefore, when reporting high Q, it is vital to use settings that result in convergence with high S-parameter accuracy.

II. Limitations of Conventional Measurement Systems

A. Vector Network Analyzer

The vector network analyzer (VNA) has its best impedance measurement performance for impedances close to 50 Ω and below, therefore, is not the most suitable instrument for the measurement of IPT coils. However, it is considered here as it is a commonly available instrument unlike the more exotic and expensive impedance analyzer.

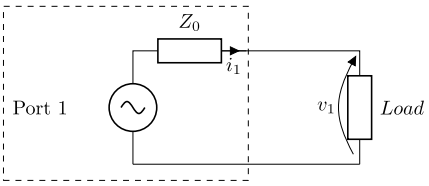

Fig. 5. Single-port measurement without resonance.

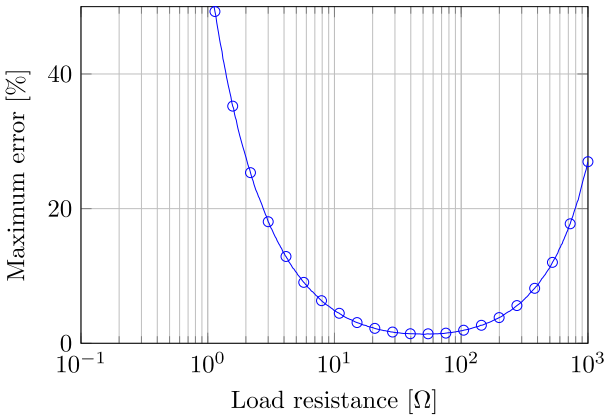

Fig. 6. Single-port real impedance maximum error R&S ZNB4 VNA, range 100 kHz–4.5 GHz.

1) Without Resonance:

$$\text{Load} = Z_{11} = Z_0\frac{1+\Gamma}{1-\Gamma}. \tag{28}$$

This simplest application of the VNA (Fig. 5), unfortunately, is not able to produce accurate results for high Q coils. The reactance of the coil causes the coil to track the outer perimeter of the Smith chart due to its high $|\Gamma\ |$. A change in R of the coil results in only very small changes in Γ. As the inductive reactance increases, the accuracy of the measured resistance falls (Fig. 5) This method has been analyzed in depth in a paper by Kuhn and Boutz who find, in practice, a VNA can report Q of below 30 with reasonable accuracy using this direct measurement method [7].

2) With Resonance: By resonating the coil to cancel its reactance, improved results are possible at resonance as the impedance no longer tracks the outer edge of the Smith chart. However, the range of impedances that can be measured using a VNA is still quite limited. To illustrate this, the maximum error in impedance measurement is plotted for the R&S ZNB4 VNA, using the manufacturer typical uncertainty specifications [19] for the frequency range of 100 kHz–4.5 GHz (Fig. 6). The measurements in this paper are toward the lower end of the frequency range; however, the performance cannot be assumed to be better than the figure. This is because the source match of the directional coupler does not extend to dc, and therefore, this is an extreme of its operation where its match is not at its best (see [20, P. 46]).

In practice, IPT coils for ISM frequencies are often in the range of 1–10 μH and 0.1–1 Ω. This results in series resonant impedances of 0.1–1 Ω and parallel resonant impedances in

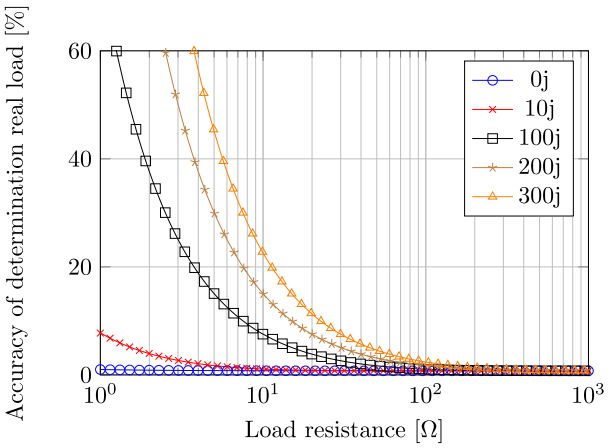

Fig. 7. E4990A impedance analyzer performance measuring real loads in the presence of reactance for the frequency range 5–10 MHz.

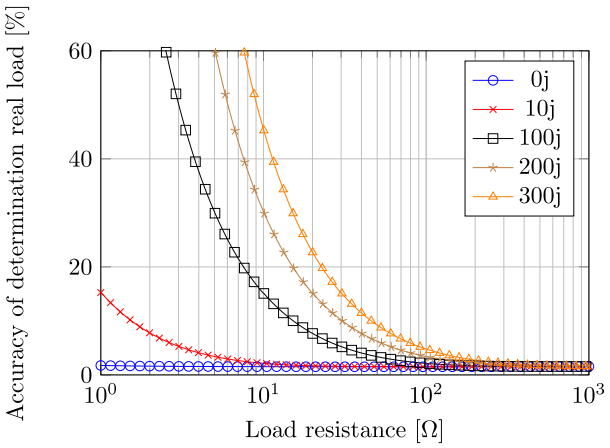

Fig. 8. E4990A impedance analyzer performance measuring real loads in the presence of reactance for the frequency range 10–120 MHz.

excess of 10 kΩ. These impedance ranges cannot be accurately resolved by the VNA using a simple method.

B. Impedance Analyzer

Impedance analyzers are four terminal measurement devices using balanced bridges or RF IV methods to determine the impedance connected between their test terminals. They can measure a much broader range of impedances far away from 50 Ω, as they measure current and voltage magnitude and phases rather than Γ with 50-Ω reference impedance as per a VNA. However, for determination of Q, the requirements placed upon the accuracy of determination of the angle of impedance are extreme, if we consider a RL series circuit with impedance, Z_{11}

$$Z_{11} = R + j\omega L \tag{29}$$

$$Q = \frac{\omega L}{R} \tag{30}$$

$$\theta = \tan^{-1}\left(\frac{\omega L}{R}\right) \tag{31}$$

$$Q = \tan\theta. \tag{32}$$

For an ideal inductor $\theta = 90°$, thus for inductors that have a high Q, a small change in the measured θ results in a great change in the measured Q. The Keysight E4990A has the greatest specified base accuracy of any impedance analyzer in its frequency range (20 Hz–120 MHz) as of 2017, with a 5% accuracy for measurement of impedance magnitude from 200 mΩ–4 MΩ, in the frequency range of 100 Hz–1 MHz.

The accuracy of this instrument (Figs. 7 and 8) from the manufacturer supplied accuracy specifications [21] has been plot in the frequency range of interest. The results show that although more capable of measuring impedance in the presence of reactance than a VNA that even in the most accurate 1-kHz–1-MHz band that the maximum Q-factors that can be reported in the most accurate region of operation are still restricted to less than 150, with reportable Q limited to around 10 in ISM bands.

In practice, these specifications have been found to be very conservative. The work of Prabhakaran and Sullivan [22] shows that Q measurements using this instrument have less than half the specified error. However, this is still insufficient to directly report high Q in ISM bands.

If the coil under test is resonated with a high Q parallel capacitor, the coil's impedance at resonance can be used to determine Q without the presence of reactance. However, as the impedance analyzer does not apply a differential excitation to the coil under test Q is overestimated at high frequencies using this method (Fig. 23).

C. Baluns

When connecting an IPT coil directly to a coaxial measurement system an unintentional conductor, caused by the electrically thick cable shield, is connected to the coil. This causes additional radiation losses as the coil approaches its self-resonant frequency [23] and also causes the resonant frequency of the coil to shift.

In an effort to show the effects of unintentional loading a single-port direct VNA measurement of a 3 turn, 310 mm outer diameter, the coil was made with and without a Mini Circuits T1-1-KK81+ balun between this and the coaxial 50-Ω test lead. The single-port direct measurement circuit (Fig. 5) is modified to include a far end balun between the coaxial cable and the coil. To better illustrate the effects of cable loading, 3-m-long test leads were used. The first self-resonance of the coil was reduced from 23.9 to 15.5 MHz by the loading of the unintentional coupling in the direct measurement without balun. Subsequent measurements using the method proposed in this paper found the coil's self-resonant frequency to be 23.8 MHz, corresponding to the direct balun measurement. Thus, it is verified that the addition of the balun removes the unintentional loading.

Baluns are generally required in systems using electrically short loop antenna to prevent currents in the outer surface of the coaxial shield. During the development of the measurement system proposed in this paper, a baluns had to be used between the loop antenna and coaxial cables. If the baluns were omitted, the measured result varied with the positioning

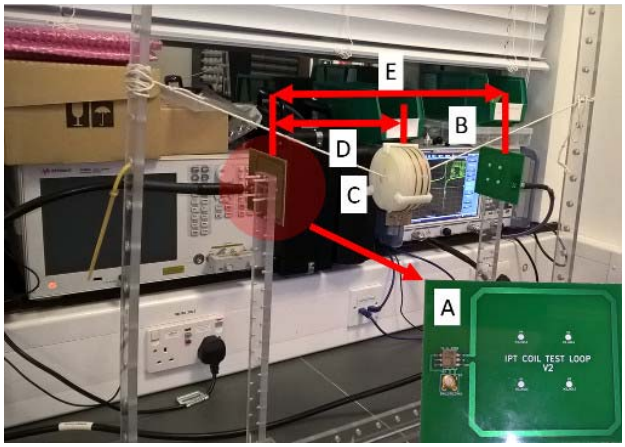

Fig. 9. Measurement system measuring a coils Q. A: Test loop connected to VNA via a Mini Circuits T1-1-KK81+ balun. B: VNA. C: Coil under test with tuning capacitors connected in parallel. D: Coil is centered between 75-mm square coupling loops. E: Distance between coupling loops.

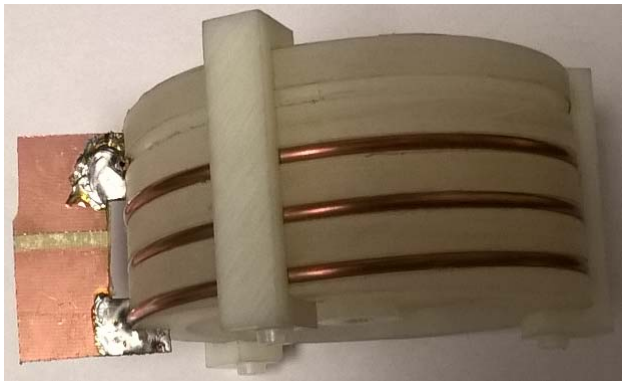

Fig. 10. Reference coil showing how PCB laminate is directly soldered to the copper tube. The tuning capacitance is soldered across the strip of laminate with copper removed.

of test cables, while with baluns, the result was stable with cable position.

III. Measurement System

The proposed measurement method is based upon those long used for determining Q of microwave cavity resonators [15]; whereby the transmission bandwidth between the two antennas coupled through a resonator is measured. The two antennas used to measure a cavity are typical an electrical monopole and a magnetic loop to minimize the coupling between the antennas. The operating frequency divided by the transmission bandwidth gives the loaded quality factor, Q_L of the cavity; where Q_L includes the energy lost to the measurement device and within the coupling mechanism. By varying their position, the coupling of the antenna to the cavity can be varied giving rise to two measurement approaches; the first is to minimize the coupling resulting in little loading but possible noise issues and the second pioneered by Kajfez [15] is to compensate for the resonator loading with relatively high coupling.

The measurement system shown in Fig. 9 is an adaptation of the cavity measurement method. To resonate, the coil capacitors (American Technical Ceramics 100A and 100B series) are soldered in parallel to the coil windings (Fig. 10); to select a new resonant frequency, the capacitor bank must be resized. As the only viable coupling mechanism in close proximity to the coil is magnetic using antenna with an electric near field is not possible and so magnetic loop antenna is used. The authors have previously used electric coupling via capacitors to the coil instead of magnetic loop coupling [24]. However, this was found to be unsuitable for the measurement of Q in the thousands as the parasitic capacitances inherent to such a measurement system result in unintentional energy loss. The antenna is connected to the VNA via baluns. As discussed in Section II-C, if these baluns are omitted, the coaxial cables will couple to each other increasing the nonresonant coupling between the loop antenna. The simpler minimal coupling resonant bandwidth method is used in preference to overdetermined methods that allow the determination of coil coupling loss. This is for a number of reasons, first, the resonant peak is not Gaussian due to a close by antiresonance that is not present in cavity measurement, second, the losses in the coupling are negligible.

A. Measurement Method

The following procedure is used to measure a coil Q at a single-frequency point. The procedure is repeated from steps 2–7 for further frequency points, determining the coil's self-capacitance requires more than one frequency point.

1) The VNA is calibrated with the reference plane located at the end of the test leads connecting to the loop antenna over the frequency range of 1–20 MHz.
2) The loop antenna is connected and the coil centrally positioned between the loop antenna. $|S_{21}|$ is measured and the transmission peak frequency located. This transmission peak should be below -30 dB, yet well discernible above the noise floor, without averaging. Adjust the loop antenna distance from the coil to satisfy this condition.
3) The VNA sweep is then adjusted to be centered upon peak and the span adjusted to just encompass the -3-dB points with respect to the peak transmission.
4) The loaded Q_L is then read from a single sweep to prevent mechanical oscillations causing distortion to the Q peak.
5) The reduction in measured Q due to the coupling to the resonator is accounted for through the relation

$$Q_0 = \frac{Q_L}{1 - 10^{\frac{|S_{21}|}{20}}}. \tag{33}$$

6) The coil's self-capacity and inductance are found by plotting $(1/\omega_0^2)$ against the measured value of the tuning capacitors for all tested frequencies. The linear line of best fit has a y-axis intercept value of the inductance and a gradient of CL. As all the measured points are used to define the line of best fit, the coil's inductance and capacitance are overdetermined.
7) After performing sufficient measurements, the coil's inductance and self-capacity are known, and therefore, the apparent loss resistance of the coil can be calculated at each frequency point.

Coil	N	s	R_{Max}	σ
Coil 1	2	2 mm	75 mm	4.74×10^7 S m^{-1}
Coil 2	3	2 mm	50 mm	5.05×10^7 S m^{-1}
Coil 3	4	5 mm	35 mm	4.86×10^7 S m^{-1}
Coil 4	3	8 mm	48 mm	4.73×10^7 S m^{-1}

Fig. 11. Reference coil physical dimensions. N is the number of turns, s is the space between the turns, and R_{Max} is the maximum outer radius of the coils. The measured and modeled inductance and capacitance of these coils can be found in Fig. 24

8) The actual loss resistance of the coil can then be obtained by subtraction of the capacitor ESR and fixture resistance at ω_0 from the apparent coil resistance. This can be used to calculate the inductor Q.

IV. Reference Coils

A set of helical reference coils has been created to compare full-wave simulation with the measurements for a wide variety of possible coil geometry. The reference coils are 3-mm external diameter tube with 0.9-mm wall thickness, the material is 99.9%+ purity copper. This copper has no guarantee of electrical conductivity, therefore the conductivity of the coils has been measured (Fig. 11). Taking a mean average of the measured conductivities yields $\sigma = 4.85 \times 10^7\,\text{S m}^{-1}$, this is less than the international annealed copper standard (IACS) of $5.8 \times 10^7\,\text{S m}^{-1}$. Despite this as long as the conductivity is taken into account during simulation, it does not affect functionality as a reference coil. When coils are used for IPT, greater efficiencies can be obtained by using IACS copper (typical at least 99.95%+ purity).

V. Measurement System Modeling

To verify the measurement system, a frequency-domain simulation model has been developed from measurement and modeling of the components of the measurement system (Fig. 12). This model is used to show system robustness and explain the observed measurement phenomenon. As the properties of virtual coils introduced to the model are exactly known, the model provides strong verification of the measurement method. This additional verification is required as it is only possible to compare the simulated and measured Q of a small number of reference coils.

A. Model

The model (Fig. 12) is composed of electrical networks that represent the coupling loops and coil linked by mutual inductances. The coupling loop is represented by a four-port network (Mini Circuits T1-1-KK81+ balun) connected to a frequency variable resistor, $R_{\text{Loop}}(\omega)$, and fixed inductance, L_{Loop} (200 nH). The frequency variable resistance of the coupling loop was estimated by simulation and its inductance by deembedding an S11 measurement (this corresponded to simulation).

The coupling loops have mutual inductance to the other coupling loop, M_{LoopLoop} (Fig. 13) and mutual inductance to the coil, M_{LoopCoil}. These inductances can be found by full-wave EM simulation or other numerical modeling. In this case, the authors used a numerical modeling method based upon finite filaments to find the mutual inductances between the coils and loops, this method will be discussed in a future paper.

The coil's self-capacitance, C_{Coil}, resistance, $R_{\text{Coil}}(\omega)$, and inductance, L_{Coil} are extracted from full-wave EM simulations of the coils.

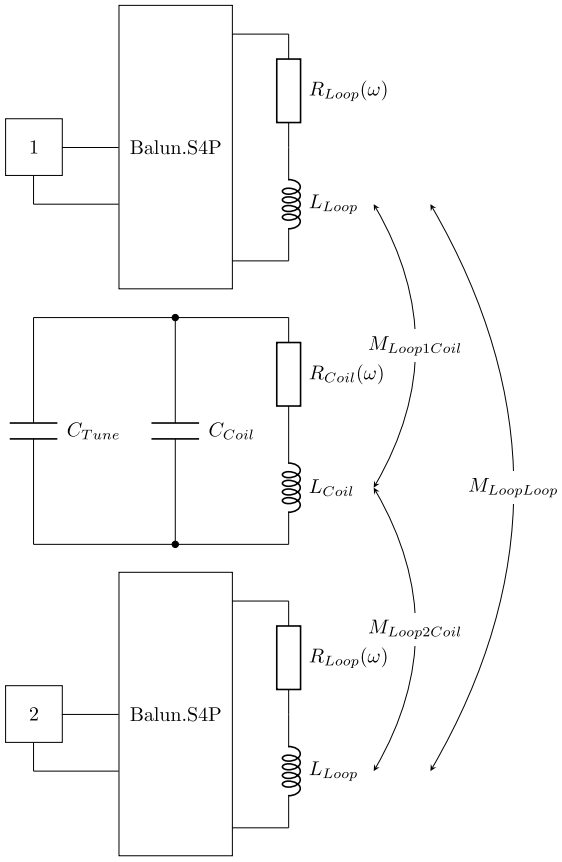

Fig. 12. Frequency-domain model of measurement system (Fig. 9)

Distance between loops	$M_{LoopLoop}$
0.09 m	6.78 nH
0.13 m	2.30 nH
0.17 m	1.12 nH
0.21 m	638 pH
0.25 m	382 pH
0.29 m	246 pH
0.33 m	172 pH
0.37 m	124 pH
0.41 m	93.1 pH
0.45 m	64.9 pH
0.49 m	54.2 pH
0.53 m	44.5 pH
0.57 m	32.1 pH
0.61 m	30.8 pH

Fig. 13. Mutual inductances of measurement system, distances correspond to stop positions of apparatus (Fig. 9).

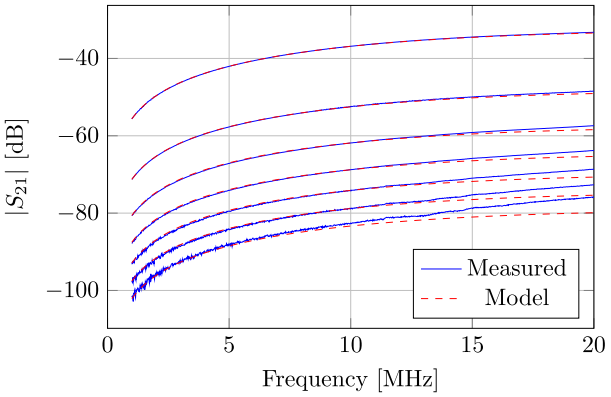

Fig. 14. Transmission magnitude comparison for distances 0.09, 0.17, 0.25, 0.33, 0.41, 0.49, and 0.57 m (greater distances have lower transmission magnitude).

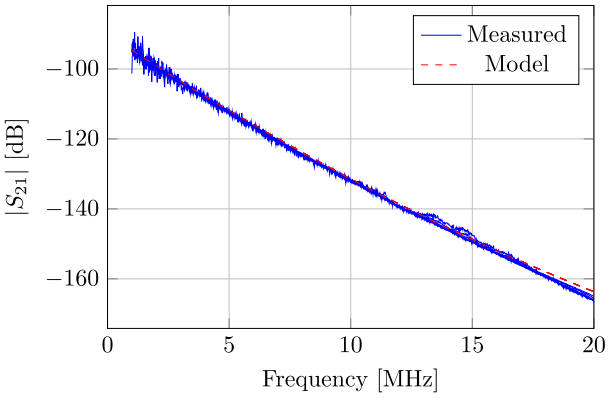

Fig. 15. Transmission phase comparison for distances 0.09, 0.17, 0.25, 0.33, 0.41, and 0.49 m.

B. Model Verification

For an accurate model, the transmission amplitude and phase between ports 1 and 2 will be the same as the measurement of the test apparatus with no coil present. Figs. 14 and 15 show the S_{21} amplitude and the phase of the measured system compared to the model of the system. The model transmission magnitude corresponds to measurement for distances between the coupling loop below 0.49 m for frequencies below 15 MHz and for distances below 0.33 m for frequencies up to 20 MHz. As the coupling is modeled as entirely magnetic, the phase does not vary with distance and corresponds until 0.49 m. It is likely the loss of relevance of the model beyond these frequencies and distances is due to a coupling mechanism that is not part of the model.

C. Distance Between Coupling Loops

The model has been utilized to show how the distance between the coupling loops influences the accuracy of the reported Q for the reference coils 1–4 (Figs. 16 and 17). Fixed tuning capacitors of 470 and 120 pF were used to resonate the coils at approximately 6.78 and 13.56 MHz, respectively. The virtual distance between the coupling loops was then varied with the coils placed centered between the two coupling loops.

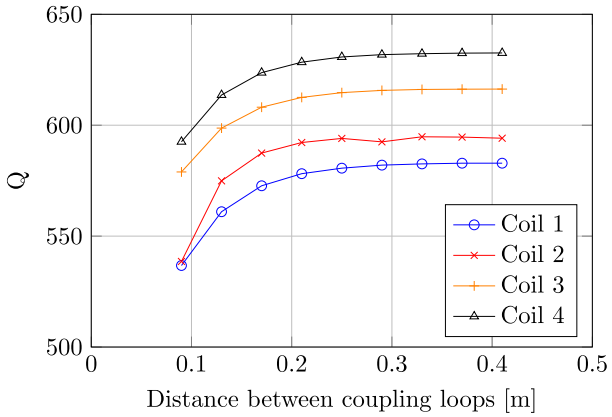

Fig. 16. Variation in Q for modeled measurement system with test loop spacing, for 470-pF tuning capacitor. Actual Q is 574, 585, 607, and 623 for coils 1–4, respectively.

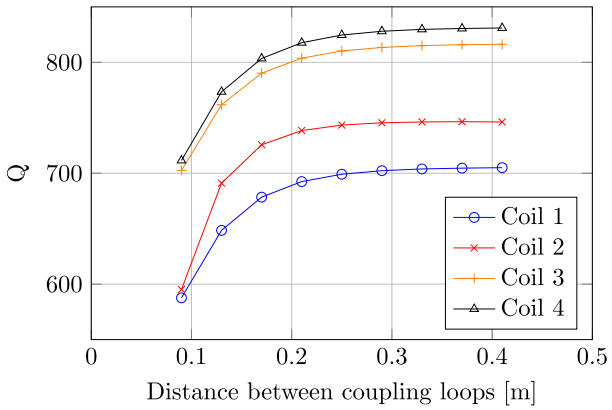

Fig. 17. Variation in Q for modeled measurement system with test loop spacing, for 120-pF tuning capacitor. Actual Q is 698, 739, 808, and 821 for coils 1–4, respectively.

The coupling even at 0.09-m distance between the coupling loops was insufficient to cause a significant shift in the coil's resonant frequency. The resonant frequency with the coupling loops was within 0.001% of the frequency without the coupling loops in all cases. Coil 1 resonates at 6.62 and 12.9 MHz, coil 2 at 6.18 and 12.1 MHz, coil 3 at 6.86 and 13.5 MHz, and coil 4 at 6.89 and 13.7 MHz.

The results (Figs. 16 and 17) show that for distance below 0.17 m, Q is underreported before converging to a value less than 1% over the actual Q for greater distances. The underreported Q can easily be rationalized by the method that is used to consider treating the coupling as lossless; as the coupling becomes more significant at closer distances, the error caused by the approximation becomes greater. Overreporting at greater distances was found to be caused by the test loop to test loop coupling, which provides an alternate transmission path that results in an antiresonance after the resonant peak. The antiresonance causes an asymmetrical reduction in the resonant peaks bandwidth, increasing the measured Q.

To illustrate the antiresonance phenomenon, the measurement of $|S_{21}|$ for coil 3 has been simulated, when the coupling loops are 0.61 m apart, with and without the coupling

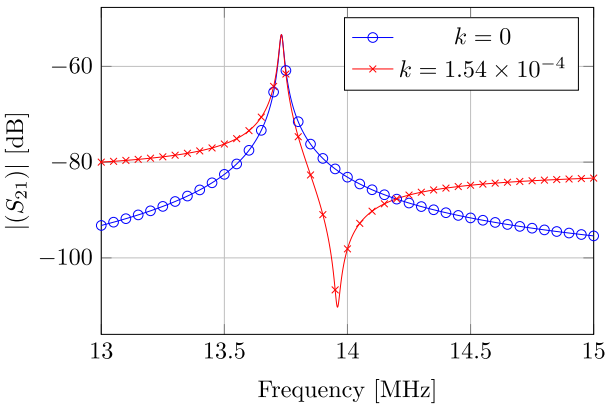

Fig. 18. Comparison of modeled measurement system with and without test loop to test loop coupling.

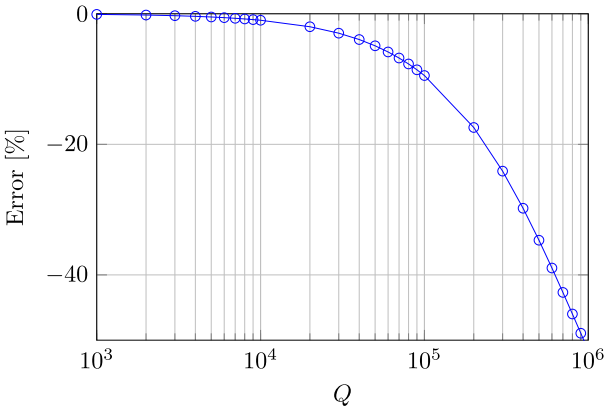

Fig. 19. Reported Q error for measurement system model with respect to resonator unloaded Q for coil 1 (with modified loss resistances) at 0.41-m test loop separation at 13.56 MHz.

factor, k, between the test loops present (1.54×10^{-4}). It can be observed that the antiresonance, which is increasing the apparent Q, is not present when this coupling is removed (Fig. 18). Although interesting and showing the utility of simulating the measurement system, this phenomenon is not liable to be the dominant source of error in the real world.

D. Modeled Measurement System Limitations

In the future, IPT coils may have Q far in excess of 1000 by the use of methods to counter the skin effect. As such, the ultimate limitations of this measurement system may be stressed by such coils. In order to find these limitations, Q of coil 1 has been varied at 13.56 MHz by adjusting the coil's effective resistance. The model of the measurement system has been configured with coupling loops 0.41 m apart, the frequency resolution of the simulation has been set to 1 Hz and the s-parameter accuracy to 1×10^{-3}.

The results (Fig. 19) show that Q of 50 000 can be measured with greater than 5% accuracy assuming the tuning capacitor is lossless or has exactly known loss. A sufficient performance for the measurement of any currently known IPT coil. The loss of accuracy at increasing Q is likely due to increasing coupling, by $Q = 50\,000$ the peak of $|S_{21}|$ is -5.22 dB. At such coupling, the approximation of lossless coupling is less valid. The approximation of lossless coupling could be avoided by removal of the antiresonance from results (allowing estimation of coupling losses) or by moving the coupling loops further apart reducing the peak $|S_{21}|$. In the real-world capacitor, Q is limited to <30 000, and therefore, the greater limitation on overall measurement system performance is the accurate knowledge of tuning capacitor Q. There are methods to measure capacitor Q [25] and if such Q were known for the resonant capacitor, rather than using estimated values of the measurement accuracy would improve. However, the measurement is quite challenging and the estimated capacitor Q is at least an order of magnitude greater than the coil Q experimentally measured in this paper. For coil Q that approaches or exceeds that of the resonant capacitor such as in this discussion of the limitations of the measurement system, it would become essential to know the actual capacitor Q.

VI. Results

A. Reference Coil Comparisons

In this section, the EM simulations conducted in CST MWS are compared to the frequency-domain simulation of the measurement system and the measurements undertaken using the transmission method. The coils are also measured using an E4990A impedance analyzer showing the spurious results that are generated using this common approach.

Correspondence for inductance between the EM simulations and measured results is excellent with less than 5% error (Fig. 24). The correspondence between the measured capacitance and the EM model is poor with error exceeding 50% for coil 3. The EM model seems to underestimate the coil's capacity, in the context of the simulator differences to reality this makes sense. The coil's capacity is a phenomenon of electrical length; if there were no phase retardation along the coil, there could be no potential difference between turns and, therefore, no capacity [26]. The simulation, having to be contained inside a computer's memory, must have a finite calculation domain. As the antenna is very electrically small, simulating the near field would require a larger practicable calculation domain, and therefore, the calculation domain has been truncated at 100 mm from the coil, and electric portions of the outer near field are not simulated correctly. Furthermore, the coils have additional capacitor mounting boards added for measurement that bring the ends of the coil (area of peak electric field) in close proximity, adding additional nonmodeled capacitance. This effect could be taken into account by measuring the capacitance of the capacitor mounting boards, or measuring the tuning capacitors when they are mounted on the mounting boards. We have decided not to focus on the coil's self-capacitance as it is not important for the performance of IPT coils in ISM bands as coils are operated far below their self-resonant frequencies to obtain high Q-factor.

For Q-factor (Figs. 20–23), the correspondence of measurement to simulation is to within 11.25% for all measured points and typically within 5% with higher frequencies where the coil is electrically longer having greater discrepancy from

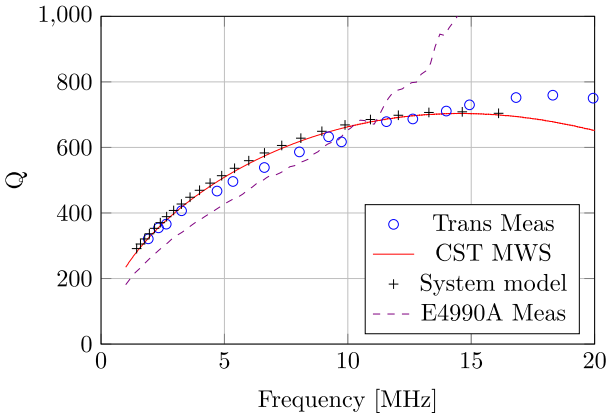

Fig. 20. Transmission modeling and measurement comparison for reference coil 1.

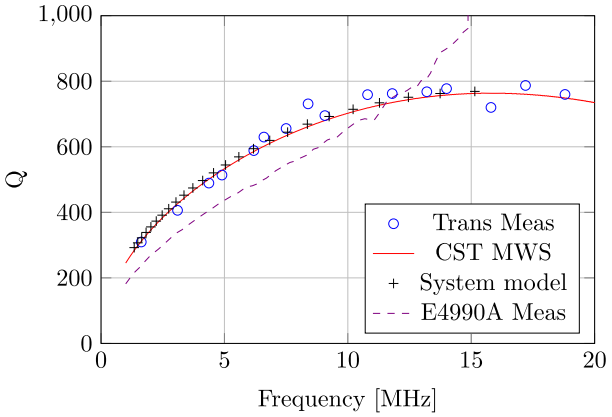

Fig. 21. Transmission modeling and measurement comparison for reference coil 2.

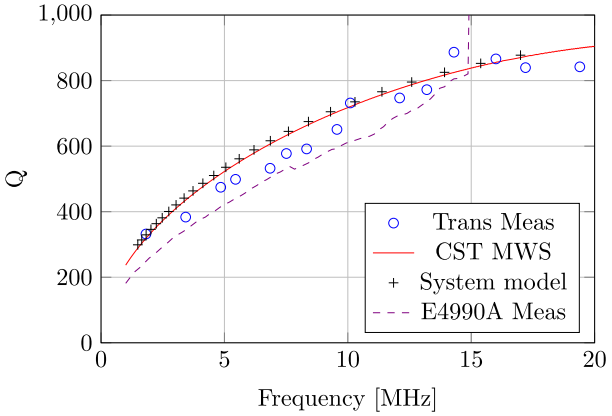

Fig. 22. Transmission modeling and measurement comparison for reference coil 3.

the simulation. The most likely cause of error at lower frequency is the use of typical values for the tuning capacitor resistance. The modeled measurement system that does not have this limitation displays practically no deviation from the EM simulator results.

The reference coils have also been measured with a Keysight E4990A impedance analyzer and 16047E test fixture

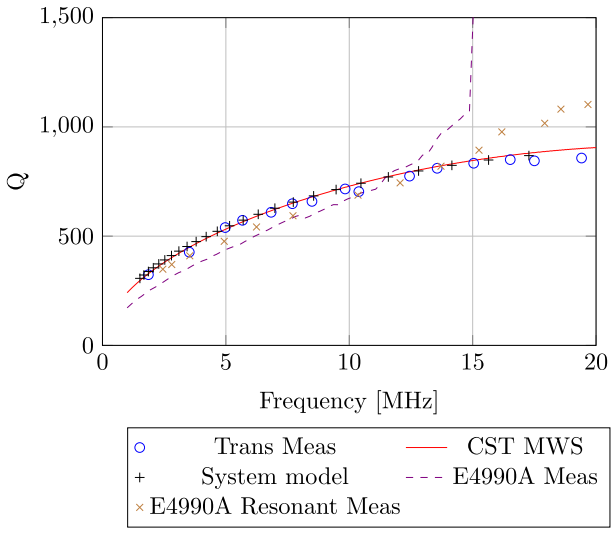

Fig. 23. Transmission modeling and measurement comparison for reference coil 4.

Coil	Inductance	Capacitance
Coil 1	1.25 µH	4.78 pF
Coil 1	1.23 µH*	5.28 pF*
Coil 2	1.44 µH	4.76 pF
Coil 2	1.40 µH*	3.83 pF*
Coil 3	1.17 µH	4.22 pF
Coil 3	1.14 µH*	1.84 pF*
Coil 4	1.11 µH	3.30 pF
Coil 4	1.10 µH*	2.14 pF*

Fig. 24. Self inductances and capacitances of reference coils (measured using measurement system), * indicates the EM simulation value.

(Figs. 20–23). These results are spurious at high frequency and show depressed Q at low frequency. The excitation supplied by this instrument is single ended as such common-mode effects will interfere with correct operation of the instrument which is evident in the results greater than 10 MHz and causes energy loss at low frequencies. When a capacitor is placed in parallel with the coil and measured with this instrument (Fig. 23 "E4990A Resonant"), the measured Q is reported with errors of up to 22%. The reduction in error compared to the direct measurement is because the measurement of a real quantity is insensitive to phase error caused by the single-ended driving of the coil. However, the result is still in error due to the impedance magnitude error.

B. Electrically Long Coil

The reference coils have <1 m of conductor length, longer coils exhibit greater radiation losses in 1–20 MHz range. An example of such a longer coil designed for maximal Q at 6.78 MHz has been measured in the same manner as the reference coils, this coil will be referred to as the long coil. The coil is designed to exhibit radiation dominated loss above 6.78 MHz and skin effect dominated loss below. The coil is loosely wound; therefore, the phase velocity is a significant fraction of the speed of light. The frequency of maximal Q is primarily adjusted by altering the length of copper pipe used

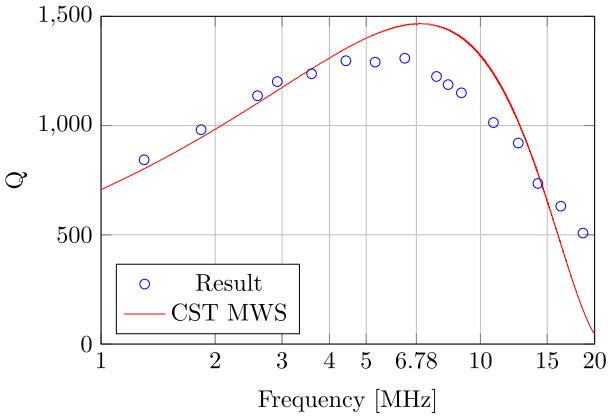

Fig. 25. Transmission modeling and measurement comparison for long coil.

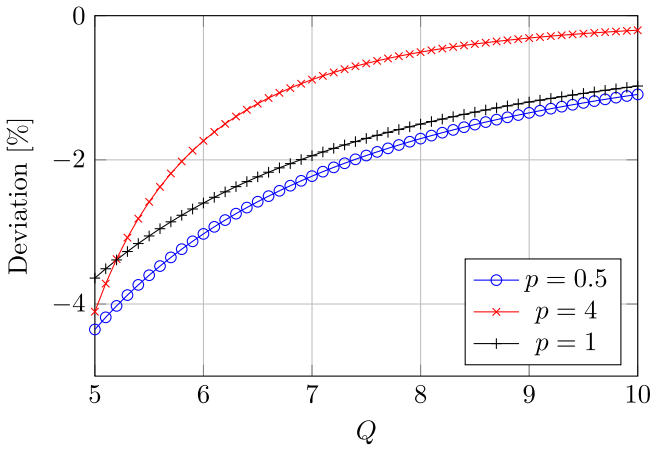

Fig. 26. Deviation of bandwidth definition of Q from energy definition for different proportionalities of R.

to construct the coil. As well as being electrically longer in the frequency range of 1–20 MHz than the reference coils, this coil is constructed using larger diameter copper tube, resulting in a greater Q; however, the tube is conventional plumbing pipe and so does not have controlled wall thickness. Therefore, there is likely to be dimensional discrepancy between the EM simulation and reality and as such this coil cannot be treated as a reference but instead is utilized as an illustration of the limitations of this measurement system.

The long coil has an outer radius of 155 mm and a turn to turn gap of 10 mm. It is composed of 5-mm outer radius copper tubes with 0.7-mm-thick walls (manufacturer specification), with a total of 3 turns. The total length of the coil is 2.83 m, the measured conductivity of the tube is $3.89 \times 10^7\,\mathrm{S\,m^{-1}}$; assuming the nominal wall thickness.

The results have been plot on a logarithmic frequency axis to show the low-frequency skin effect loss dominated region (ESR $\propto \omega^2$) and the high-frequency radiation loss dominated region (ESR $\propto \omega^4$) (Fig. 25). Very good correspondence to simulation is observed in the low-frequency region. However, the slope of high-frequency region is only $\omega^{-1.3}$ showing far less than the expected radiation loss. This could be caused by conducting the experiment in a nonanechoic environment with many metallic objects within the near field. However, this region of operation is not very interesting for IPT as it is below the point of peak efficiency, and there is a significant electric field close to the coils, which interacts more strongly with the typical matter than the magnetic field.

VII. Conclusion

A measurement system and methods for finding the equivalent electrical parameters of megahertz frequency air-core IPT coils have been presented. The system is capable of measuring coil Q in excess of 1000 in the range of 1–20 MHz. To produce measurement results that match simulation, the fitting of electrical models to results and the definitions of Q have been examined. Furthermore, practical measurement challenges such as the conversion between unbalanced and balanced modes are addressed. As a result of examining and resolving these issues, the system measures coil Q to typically within 5% of simulation. The greatest source of error appears to be the lack of suitable apparatus to measure the loss resistance of the resonant capacitor.

Coil inductance is also resolved accurately by this measurement system; however, the authors were unable to verify that coil capacitance is accurately resolved beyond correct extraction from the modeled measurement system.

The frequency-domain model of the measurement system shows insensitivity to exact setup as long as simple guidelines on test loop positioning are observed. Furthermore, this model shows that the ultimate accuracy of this system if the resonant capacitor loss was known could be as good as 1% for $Q = 1000$.

As the developed measurement system requires soldering capacitors manually to select each frequency point, the authors in the future aim to develop measurement systems that can switch tuning capacitors without loss of accuracy. This would allow the coil to be measured automatically.

Appendix
Q Definition Equivalence With Dispersion

As previously discussed, there are two definitions of Q (energy and bandwidth definitions) that are nonidentical, furthermore, the coils are dispersive. In the lower frequency regime $R \propto \omega^{0.5}$ (skin effect dominated), while in the higher frequency regime $R \propto \omega^4$ (radiation loss dominated). As a result over the coils resonant bandwidth, $\Delta\omega$, the coils Q under the energy definition will have changed.

To test the equivalence of these definitions under dispersive conditions, the following equation is used to represent the coils resistance in the coil model (Fig. 2):

$$R(\omega) = k\omega^p \tag{34}$$

where k is a constant defining the Q-factor at ω_0 and p is the power of proportionality for the dominant effect. By numerical modeling, the error between the energy definition of Q methods that use the resonator bandwidth has been plot (Fig. 26) for constant R with respect to frequency and the two common proportionality's.

Significant differences between the two definitions only occur at low Q, where the bandwidth definition underreports Q. Even for the most dispersive modeled case, the error is small for the high Q coils used in IPT systems, and mostly attributable to the difference between the two definitions. As IPT coils are expected have $Q \gg 10$, the effects of the coil's dispersion and difference in definitions of Q can be safely ignored.

REFERENCES

[1] S. Y. R. Hui, W. Zhong, and C. K. Lee, "A critical review of recent progress in mid-range wireless power transfer," *IEEE Trans. Power Electron.*, vol. 29, no. 9, pp. 4500–4511, Sep. 2014.

[2] Y. Akuzawa, Y. Ito, T. Ezoe, and K. Sakai, "A 99%-efficiency GaN converter for 6.78 MHz magnetic resonant wireless power transfer system," *J. Eng.*, vol. 2014, no. 10, pp. 598–600, Oct. 2014.

[3] C.-C. Hou, W.-P. Chang, Y.-H. Teng, and K.-J. Lee, "Planar spiral coils for inductive power transfer systems," in *Proc. IEEE 2nd Int. Future Energy Electron. Conf. (IFEEC)*, Nov. 2015, pp. 1–6.

[4] M. Fu, T. Zhang, X. Zhu, and C. Ma, "A 13.56 MHz wireless power transfer system without impedance matching networks," in *Proc. IEEE Wireless Power Transf. (WPT)*, May 2013, pp. 222–225.

[5] S. Aldhaher, D. C. Yates, and P. D. Mitcheson, "Design and development of a class EF_2 inverter and rectifier for multimegahertz wireless power transfer systems," *IEEE Trans. Power Electron.*, vol. 31, no. 12, pp. 8138–8150, Dec. 2016.

[6] M. Pinuela, D. C. Yates, S. Lucyszyn, and P. D. Mitcheson, "Maximizing DC-to-load efficiency for inductive power transfer," *IEEE Trans. Power Electron.*, vol. 28, no. 5, pp. 2437–2447, May 2013.

[7] W. B. Kuhn and A. P. Boutz, "Measuring and reporting high quality factors of inductors using vector network analyzers," *IEEE Trans. Microw. Theory Techn.*, vol. 58, no. 4, pp. 1046–1055, Apr. 2010.

[8] B. H. Waters, B. J. Mahoney, G. Lee, and J. R. Smith, "Optimal coil size ratios for wireless power transfer applications," in *Proc. IEEE Int. Symp. Circuits Syst. (ISCAS)*, Jun. 2014, pp. 2045–2048.

[9] R. Bosshard, J. W. Kolar, J. Mühlethaler, I. Stevanović, B. Wunsch, and F. Canales, "Modeling andη-α-Pareto optimization of inductive power transfer coils for electric vehicles," *IEEE J. Emerg. Sel. Topics Power Electron.*, vol. 3, no. 1, pp. 50–64, Mar. 2015.

[10] D. H. Kim, J. Kim, and Y. J. Park, "Optimization and design of small circular coils in a magnetically coupled wireless power transfer system in the megahertz frequency," *IEEE Trans. Microw. Theory Techn.*, vol. 64, no. 8, pp. 2652–2663, Aug. 2016.

[11] M. Zargham and P. G. Gulak, "Maximum achievable efficiency in near-field coupled power-transfer systems," *IEEE Trans. Biomed. Circuits Syst.*, vol. 6, no. 3, pp. 228–245, Jun. 2012.

[12] C. R. Paul, *Inductance Loop Partial*. 1st ed. Hoboken, NJ, USA: Wiley, 2011.

[13] F. Grover. Inductance Calculations: Working Formulas and Tables. New York, NY, USA: Dover, 2004. [Online]. Available: https://books.google.co.uk/books?id=K3KHi9lIltsC

[14] S.-H. Lee and R. D. Lorenz, "Development and validation of model for 95%-efficiency 220-W wireless power transfer over a 30-cm air gap," *IEEE Trans. Ind. Appl.*, vol. 47, no. 6, pp. 2495–2504, Nov./Dec. 2011.

[15] D. Kajfez, *Q Factor Measurements Using MATLAB*, 1st ed. Norwood, MA, USA: Artech House, 2011.

[16] Z. Pantic and S. Lukic, "Computationally-efficient, generalized expressions for the proximity-effect in multi-layer, multi-turn tubular coils for wireless power transfer systems," *IEEE Trans. Magn.*, vol. 49, no. 11, pp. 5404–5416, Nov. 2013.

[17] R. W. V. Duzer, *Fields Waves Communication Electron.*, 3rd ed. Hoboken, NJ, USA: Wiley, 1993.

[18] H. J. R. C. Johnson, *Antenna Engineering Handbook*, 2nd ed. New York, NY, USA: McGraw-Hill, 1984.

[19] *RS ZNB Vector Network Analyzer Specifications*. Rohde Schwarz, Munich, Germany, 2014.

[20] J. P. Dunsmore, *Handbook of Microwave Component Measurements: With Advanced VNA Techniques*. Hoboken, NJ, USA: Wiley, 2012.

[21] *Keysight technol. E4990A Impedance Analyzer 20 Hz to 10/20/30/50/120 MHz Data Sheet*, Keysight, Santa Rosa, CA, USA, 2015.

[22] S. Prabhakaran and C. R. Sullivan, "Impedance-analyzer measurements of high-frequency power passives: Techniques for high power and low impedance," in *Proc. Conf. Rec. IEEE Ind. Appl. Conf. 37th IAS Annu. Meeting*, vol. 2, Oct. 2002, pp. 1360–1367.

[23] O. Bushueva, C. Viallon, A. Ghannam, and T. Parra, "On-wafer measurement errors due to unwanted radiations on High-Q inductors," *IEEE Trans. Microw. Theory Techn.*, vol. 64, no. 9, pp. 2905–2911, Sep. 2016.

[24] J. Lawson, M. Pinuela, D. C. Yates, S. Lucyszyn, and P. D. Mitcheson, "Long range inductive power transfer system," *J. Phys., Conf. Ser.*, vol. 476, no. 1, 2013, Art. no. 012005. [Online]. Available: http://stacks.iop.org/1742-6596/476/i=1/a=012005

[25] M. Ingalls and G. Kent, "Measurement of the characteristics of high-Q ceramic capacitors," *IEEE Trans. Compon., Packag., Manuf. Technol.*, vol. CPMT-10, no. 4, pp. 487–495, Dec. 1987.

[26] G. Grandi, M. K. Kazimierczuk, A. Massarini, and U. Reggiani, "Stray capacitances of single-layer solenoid air-core inductors," *IEEE Trans. Ind. Appl.*, vol. 35, no. 5, pp. 1162–1168, Sep./Oct. 1999.

James Lawson received the M.Eng. degree in electrical engineering and the Ph.D. degree from Imperial College London, London, U.K., in 2012 and 2017, respectively. His doctoral thesis was focused on high-frequency electromagnetic links for wireless power transfer.

He is currently an Electronic Engineer with the Nuclear Physics Group, STFC Daresbury Laboratory, Warrington, U.K. His current research interests include impedance spectroscopy, wireless power transfer, and high-frequency power conversion.

David C. Yates (M'03) received the M.Eng. degree in electrical engineering and the Ph.D. degree from Imperial College London, London, U.K., in 2001 and 2007, respectively. His doctoral thesis was focused on ultralow-power wireless links.

He is currently a Research Fellow with the Control and Power Group, Department of Electrical and Electronic Engineering, Imperial College London. His current research interests include converters and magnetics for wireless power transfer and ultralow-power RF circuits for sensor networks.

Paul D. Mitcheson (SM'12) received the M.Eng. degree in electrical and electronic engineering and the Ph.D. degree in micropower motion-based energy harvesting for wireless sensor networks from Imperial College London, London, U.K., in 2001 and 2005, respectively.

He is currently a Professor of electrical energy conversion with the Control and Power Research Group, Electrical and Electronic Engineering Department, Imperial College London. His research has been supported by the European Commission, Engineering and Physical Sciences Research Council, and several companies. His current research interests include energy harvesting, power electronics, and wireless power transfer to provide power to applications in circumstances where batteries and cables are not suitable

Dr. Mitcheson is a Fellow of the Higher Education Academy and is on the Executive Committee of the U.K. Power Electronics Centre.